Transformation of Industrial By-Products into Composite Photocatalytic Materials

Eleni Katsika[1*], Maria Volioti[1], Vayos G. Karayannis[2], Angeliki Moutsatsou[1]

[1] Laboratory of Inorganic and Analytical Chemistry, School of Chemical Engineering, National Technical University of Athens (NTUA), 15780 Zografou, Athens, Greece
[2] Department of Chemical Engineering, University of Western Macedonia (UOWM), 50100 Kozani, Greece
* Corresponding author, e-mail: vkarayan62@gmail.com

Abstract

The transformation of both calcareous and siliceous Greek power station by-products (lignite ashes) into novel composite materials with photocatalytic properties for environmental application was investigated. Particularly, a comparison between the development of coated ceramic substrates and the modification of ash surfaces is attempted. Specifically, a) the sintering process (1000 °C, 2 h) of both fly and bottom ash (either calcareous or siliceous) for their conversion into compacted ceramic substrates coated with TiO_2 slurry and then further thermally treated (500 °C, 1 h) to acquire TiO_2 film consistency onto the ceramic substrate and b) the process of TiO_2 precipitation on lignite ash surfaces in acidic solution after neutralization, and estimation of the TiO_2 percentage, are compared. The microstructures obtained were examined by XRD and SEM-EDX analysis. Vickers microhardness was also determined for the ceramic microstructures, with satisfactory results (up to 356HV). The energy gap measurements of the coatings were found to be between 3.02eV and 3.17eV, which is located between the energy gap of anatase (3.23eV) and rutile (3.02eV). The coating mass was about 0.059 g/cm^2. The photocatalytic activity under visible and UV irradiation was investigated in aqueous solutions of methylene blue and methyl orange organic dyes, with encouraging results. A main advantage of the processes proposed is the immobilization of TiO_2 onto largely available secondary resources, which can lead to production of value-added 'green' photocatalysts for the treatment of industrial effluents in the framework of circular economy.

Keywords

industrial by-product, transformation, photocatalytic material, composite, circular economy

1 Introduction

The transformation of industrial by-products, considered as useful secondary raw materials rather than as wastes, into 'green' products can contribute to environmental protection, resources conservation and cost reduction. Nowadays, the environmental legislation strongly encourages manufacturers to utilize industrial by-products, under specific limitations.

Particularly, the processing, upgrading and valorization of Fly Ash (FA) and Bottom Ash (BA), which are produced in massive quantities from coal/lignite combustion for power generation, is currently of increasing importance [1-6]. The recycling and transformation of ashes into value-added materials represents an alternative to disposal and could provide significant economic and environmental benefits. So far, the global average utilization rate has been estimated to be nearly 25 % of FA production [7].

In Greece, approx. 8 million tons of ashes are annually generated from lignite combustion in power stations. 80 % of this amount comes from Northern Greece (Region of Western Macedonia) where the main lignite deposits of the country are located, whereas the rest from Megalopolis (Region of Peloponnese in Southern Greece). The use of FA (mainly in cement industry) still remains to about 20 % of the annual production, while the rest is directly discharged into ponds and landfills. So, utilization of FA must be raised to avoid environmental impacts [8-10].

Research efforts focus on the addition of FA in construction materials including conventional cement-based products as well into clayey mixtures at different combinations and proportions for manufacturing ceramic, glass-ceramic and geopolymeric materials, due to FAs interesting physicochemical properties [11-18]. Moreover, the utilization of

FA to act as synthetic zeolite for remediation of soils contaminated by heavy metals is reported in other study [19]. Also, FA has been successfully tested as a low-cost adsorbent to remove Cu and Cd ions from aqueous solutions [20]. Recent research interest is placed on applications of fly ash for CO_2 capture and utilization [21]. Especially, lignite ashes can be considered as attractive secondary resources for use in environmental applications of heterogeneous catalysis due to their aluminosilicate content. This can provide a cost-effective and environment-friendly alternative for the beneficial utilization of ashes [2, 22].

In order to convert by-products such as lignite ashes into photocatalysts, titanium oxide (TiO_2) can be considered as an appropriate additive, as it is the most common, efficient and usable semiconductor in photocatalytic oxidation, with significant advantages and excellent physicochemical and photocatalytic properties in comparison to the other semiconductors. TiO_2 in the crystalline phase of rutile (tetragonal) is the most stable form compared to anatase (tetragonal) and brookite (orthorhombic) phases that are metastable and can be transformed to rutile phase under ~750 °C. Anatase and rutile TiO_2 are most often reported as photocatalysts: recent results demonstrated that a mixed form of rutile and anatase TiO_2 displayed enhanced photocatalytic ability, since the transfer of electrons from anatase to a lower-energy rutile electron-trapping site in mixed-phase could reduce their combination rate of charge carriers in anatase TiO_2 and effectively create catalytic "hot spots" [23, 24].

Furthermore, other inorganic by-products have been studied as substrates for their photocatalytic ability. An example is blast furnace ash as well as the ash of agricultural by-products [25, 26]. Techniques that have been investigated for depositing TiO_2 on the surface of materials of this category are: the co-grinding at high temperatures, the sol-gel method, precipitation, thermal spraying, deposition, pulsed power, and other [27, 28].

The present research focuses on the comparison of two different processes of TiO_2 immobilization onto lignite ashes for their transformation into novel photocatalysts:

1. Ceramic substrates are prepared starting from either siliceous or high-calcium ash and, then, their surfaces are activated, by coating them with TiO_2 slurry: the microstructures obtained are studied in relation to TiO_2 coating, drying and thermal treatment conditions. Apart from eliminating the obstacles encountered with the use of the catalyst in the form of particle dispersions and suspensions (need for solid-liquid separation after treatment, particle aggregation etc.), another significant advantage of the whole process of photocatalyst immobilization is the potential for photocatalytic decomposition of persisting (hardly biodegradable or even non-biodegradable) pollutants. The effect of iron oxides existing in lignite fly ash in small quantities on the photocatalytic activity of TiO_2 is also discussed.

2. Siliceous and high-calcium lignite ash (fly and bottom ash) are directly surface activated by TiO_2 precipitation onto their surface: the product microstructure is studied according to the parameters of TiO_2 precipitation in acidic solution after neutralization and hydrolysis. Moreover, the effect of different mineralogical phases and physicochemical properties of ashes on the rate and form of the resulting TiO_2 or even the reaction with components of the ashes is investigated. The research aims to extend the field of ash application for further treatment of liquid wastes such as dye-house, electroplating effluents etc., by studying the effect of surface coating ashes of different particle sizes (as received and < 45 μm) and for 1h ageing time. The determination of the ash physicochemical characteristics (specific surface area, specific weight, pH) are necessary for the selected technique of transformation/modification.

2 Materials and methods
2.1 Materials
Fly ash (FAAD) was obtained from the electrostatic precipitators of lignite-fed Agios Dimitrios lignite power plant (Region of Western Macedonia). It is a fine powder highly-calcareous (Class-C according to ASTM C 618). On the other hand, Megalopolis fly ash (FAM) is strongly siliceous: almost half of it consists of SiO_2 with lesser amounts of Ca-bearing species also present (barely a Class-C ash).

Bottom ash is also formed during lignite firing in Agios Dimitrios and Megalopolis units (BAAD and BAM respectively), and is removed from the bottom of dry boilers. It is a granular material much coarser than FA.

All types of ash were evaluated in terms of their chemical composition by means of X-ray fluorescence (XRF, X-Lab 2000 EDAX, Siemens D-500), loss on ignition (ASTM D7348), pH (ISO 6588) and free CaO content (CaOf-ASTM C151). Mineralogical analysis was performed by X-ray Diffraction, while the particle size distribution was determined using Malvern MasterSize-S by applying the wet dispersion method in water.

The chemical content, the physicochemical properties and the mineralogical composition of the ashes are given in Tables 1 and 2, and Fig. 1 respectively. The main crystalline phases detected in the Agios Dimitrios ashes (FAAD and BAD) are gypsum ($CaSO_4.2H_2O$), quartz (SiO_2), lime (CaO), calcite ($CaCO_3$), and a-hematite (Fe_2O_3). On the other hand, the main mineralogical phases of the Megalopolis ashes (FAM and BAM) are quartz (SiO_2), silicon oxide (SiO_2) and iron oxide (Fe_2O_3).

2.2 Preparation of coated ceramic substrates

Disc-shaped compacted specimens (13 mm diameter and 3mm width) were formed each time from FAAD and FAM by uniaxially cold pressing in a stainless-steel die using a hydraulic press (Specac, 15011), and then were consolidated employing sintering procedure in a laboratory chamber programmable furnace (Thermoconcept, KL06/13). A temperature lower than the vitrification point of the ashes was selected as a peak sintering temperature (1000 °C), with 2h soaking time. Finally, the sintered specimens were gradually cooled to ambient temperature into the furnace. Then the specimen surfaces were coated with TiO_2 slurry (8 % TiO_2, 89.9 % water and 2.1 % disruptive factor), and subsequently were exposed at 500 °C for 1h to acquire TiO_2 consistency on the ceramic substrate.

The obtained microstructures were thoroughly examined by XRD and SEM-EDAX (Jeol, JSM-6400). Also, the difference of the ceramic substrate microstructures after the second heating treatment was examined for the surface consistency. The shrinkage of the samples was calculated as the volume change (%) upon sintering. The apparent density was determined according to the Archimedes principle using a specific apparatus (Shimadzu, SMK401-AUW220V). Vickers microhardness was measured with a load of 50 g and a dwell time of 15 s (Wilson Instruments, Mode 402MVD, Knoop Vickers Tester). In order to enable reliable comparisons, mean microhardness values over five valid indentations per specimen were calculated. Moreover, the average surface roughness of the coated substrates was determined (Bruker, Nano Surfaces Division, Countour GT, Vision 64 Software).

2.3 Preparation of coated lignite ash powders

For the direct surface coating of lignite ashes with TiO_2, the technique of hydrolysis and simple precipitation was used. This choice was established taking into consideration the physicochemical characteristics of the ashes and the low cost of the process in relation with the price

Table 1 Chemical content of FAAD, BAAD, FAM and BAM

(%)	FAAD	BAAD	FAM	BAM
SiO_2	30.16	48.63	49.54	50.23
Al_2O_3	14.93	21.62	19.25	20.40
Fe_2O_3	5.10	7.29	8.44	9.35
CaO	34.99	6.83	11.82	7.90
MgO	2.69	2.75	2.27	2.30
SO_3	6.28	2.78	3.91	1.89
$N_{a2}O$	1.01	0.89	0.53	0.45
K_2O	0.40	2.97	1.81	1.98
LOI	3.95	5.34	2.10	5.78
	*CaO_f: 10.87%		*CaO_f: 5.95 %	

Table 2 Physicochemical properties of the ashes

	pH	Particle size distribution (µm)		Specific Weight (g/cm^3)
		D(v, 0.5)	D(v, 0.9)	
FAAD	12.5	30.92	98.28	2.67
BAAD	8.5	85.93	199.08	2.74
FAM	11.8	98.92	199.87	2.62
BAM	8.9	97.92	208.14	2.73
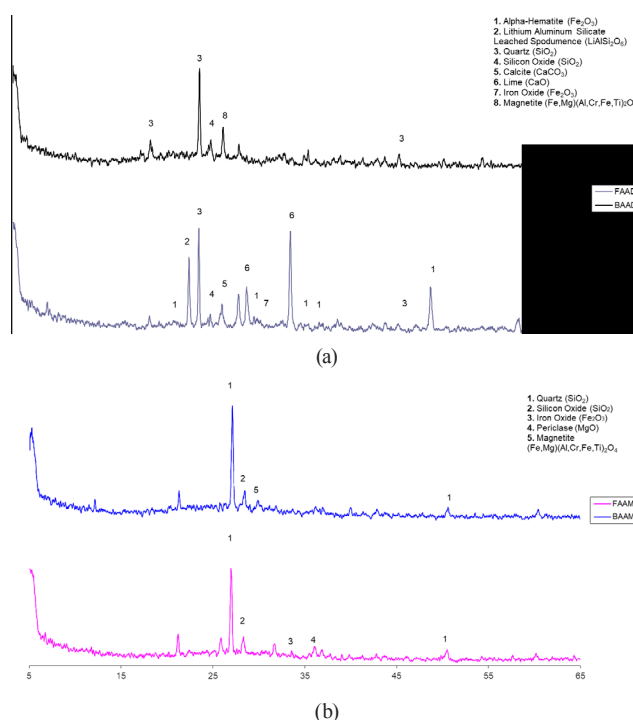
Fig. 1 Mineralogical composition of the (a) FAAB and BAAD and (b) FAM and BAM ashes.

of the raw material. Acidic solution of $TiCl_4$ ($TiCl_4/HCl$ 1:2.5 moles) was prepared, in order to avoid the formation of orthotitanate acid. Then 18 g of lignite ash (particle size as-received and after grinding to <45 µm) was

added under stirring in the solution. Moreover, for the neutralization of the solution, 81.5 mL 2M NH_4HCO_3 was added. Then the final solution was subjected to 1h ageing time. The product was filtered, dried for 24h and sintered at 500 °C for 2 h. Its microstructure was examined by X-ray diffraction (Siemens D-500) and by Scanning Electron Microscopy (FEI Quanta 200 coupled with an EDAX detector).

2.4 Photocatalytic activity

The photocatalytic activity of the composite materials produced was evaluated in the decolorization of two organic dyes (potential pollutants) as a function of time, under visible (daylight) or UV (UV-A) irradiation. The dye used in the experiments under visible irradiation was Methylene Blue (MB), a cationic dye with molecular formula $C_{16}H_{18}ClN_3S$, while the dye used under UV irradiation was Methyl Orange (MO), an anionic dye with molecular formula $C_{14}H_{14}N_3NaO_3S$. The selection of MB and MO was made because they are commonly used as standard pollutant compounds in many studies, and their absorption is easy to detect through spectrophotometry measurements. Indeed, organic dyes are important and common effluents of textile industry [29, 30].

Synthetic aqueous solutions of MB and MO with initial concentrations of 0.4×10^{-5} M and 1.7×10^{-5} M respectively were prepared, by dissolving dye powder (Fluka and Merck respectively) in distilled water. The solutions were saturated in oxygen by bubbling O_2 in the solution for 1.5 h prior to use. The photocatalytic process was carried out in round-bottom photocatalytic Pyrex glass cells that are transparent to wavelengths above 320 nm. The activated disc-shaped substrates were cut in surface areas of about 1 cm^2 and inserted in the photocatalytic cell with 5 ml of the dye solution. In the case of the e lignite ashes powders coated with TiO_2, quantity of 5 mg was inserted in the cell along with 5 ml of the dye solution.

The laboratory system used for the irradiation of the cells containing the samples was equipped with four parallel OSRAM L15W/865 LUMILUX Cool Daylight tubes for the experiments under visible light. For UV irradiation, two experiment series were carried out, using either SYLVANIA blacklight 368 F15W/T8/BL368 tubes with maximum emission at 368 nm, either SYLVANIA blacklight blue F15W/BLB-T8 tubes with maximum emission at 350 nm. All photocatalytic experiments were performed under continuous magnetic stirring, while pH and temperature values of the solutions were maintained constant.

The decomposition of the dye pollutants as a function of time and the decolorization rate were spectrophotometrically determined (UV-VIS Spectrophotometer HITACHI U-2001) by recording the absorption spectra of samples taken out at specific time intervals and measuring the change in intensity of the characteristic peak at the maximum absorption wavelength of the dyes $(\lambda_{max,MB} = 664.0$ nm, $\lambda_{max,MO} = 463.0$ nm$)$. Then, the dye decomposition efficiency was determined using the following equation:

$$\text{Efficiency}(\%) = \frac{(C_0 - C)100}{C_0},$$

where: C_0 is the initial concentration of dye solution and C is the final concentration after illumination by visible or UV light.

3 Results and discussion

XRD spectra of the coating of the ceramic substrates under different thermal treatment conditions are presented in Fig. 2. It can be seen that the main mineral phases of all coated surfaces are anatase and rutile.

The mineralogical analysis of the ceramic substrates obtained either from FAAD or FAM fly ash is shown in Fig. 3 (a) and 3 (b) respectively. For the ceramic substrates made of FAAD, the main phases are anhydrite and quartz. In the non-sintered specimen (Fig. 3 (a), A), the intensity of the peak associated with lime (CaO) predominates. The ash specimens sintered up to 1000 °C (Fig. 3 (a), B) as well as those further thermally treated after coating (Fig. 3a, C) exhibit different mineralogical compositions, and after the thermal treatment, gehlenite, anhydrite and quartz are the main phases. For FAM non-sintered specimens, quartz (SiO_2) is the predominant phase (Fig. 3 (b), A), while quartz, cyanite and gehlenite are detected after sintering the specimens up to 1000 °C (Fig 3 (b), B). The same phases appear in the substrates further thermally treated after coating (Fig. 3 (b), C). Therefore, it can be concluded that the mineralogical phases
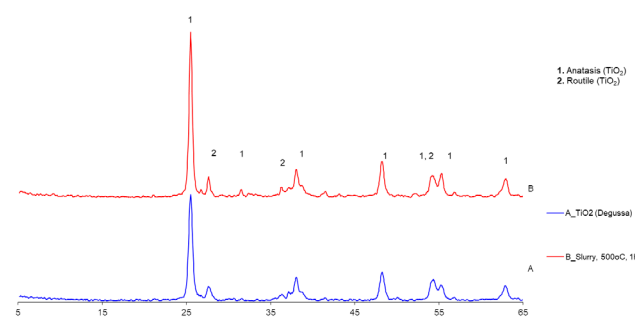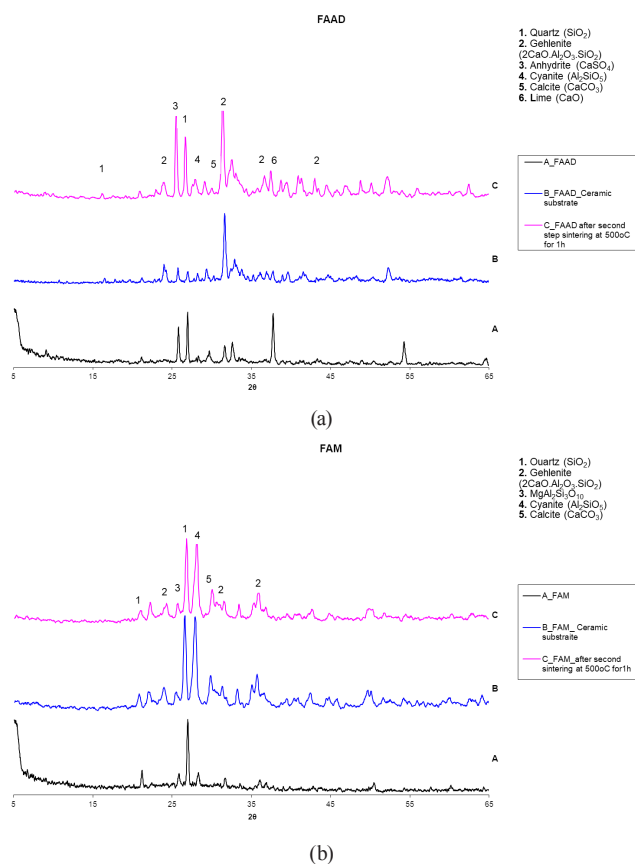

Fig.2 XRD spectra of the coating of the ceramic substrates: (A) TiO_2 (Degussa) and (B) sintered at 500 °C for 1h.
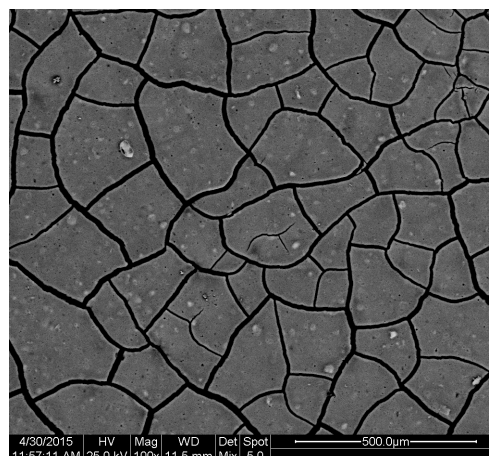
Fig. 3 XRD spectra of the ceramic substrates (a) FAAD and (b) FAM:(A) non-sintered, (B) after sintering at 1000 °C and (C) after further thermal treatment of the coated substrates at 500 °C for 1h.

Fig. 4 SEM micrographs of the surface coating of ceramic substrates thermally treated for 1h at 500 °C.

Table 3 % TiO_2 precipitated on ash surfaces

	FAAD	BAAD	FAM	BAM
As received	20.13 %	55.97 %	31.08 %	40.94 %

detected after further heating of the coated substrates were already generated during the main sintering process and no further mineralogical change is recorded.

SEM micrographs of the ceramic substrate surface coating after thermal treatment at 500 °C for 1h is provided in Fig. 4.

Surface coating cracks are clearly seen on the ceramic substrates due to the removal of water and degradation of the organic compounds of the slurry during heating. The surface roughness of the TiO_2-coated substrates after their thermal treatment at 500 °C was found to be 15.8 Sa (μm) for FAAD and 5.81 Sa [μm] for FAM. The apparent density of the sintered substrates lies in the range of 1.17-1.78 g/cm³. The Vickers microhardness for the non-sintered specimens is 230 HV and raises up to 469 HV after sintering.

On the other hand, the surface of lignite ashes is coated with TiO_2 of an amount of 20 to 56 %, as it was deduced by weight measurements conducted. The results are presented in Table 3. It can be noted that bottom ashes seem to have greater coating rates, which can be mainly attributed to their higher porosity.
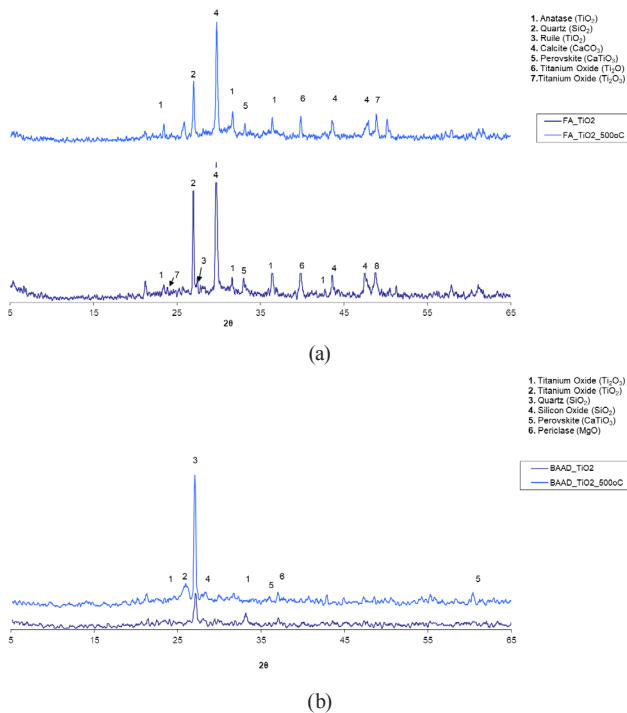
In Fig. 5, XRD spectra of non-sintered and sintered (500 °C, 2h) coated FAAD (particle size as received, ageing time 1h) and BAAD (as received - ageing time 1h) high-Ca ashes are shown.

It can be observed (Fig. 5) that the crystalline phase of calcite is decomposed upon heating and the phases that obviously predominate in the sintered materials are quartz (SiO_2), calcium titanium oxides ($CaTiO_3$, $Ca_2Ti_5O_{12}$), as well as anatase and rutile (TiO_2).

Experiments performed with the siliceous ashes at the received particle size and 1h ageing time of the precipitate (Fig. 6, XRD spectra of 500 °C, 2 h sintered (a) coated FAM, (b) BAM) revealed a decomposition of calcium titanium oxide ($CaTiO_3$) with temperature increase and main crystalline phases present are quartz (SiO_2), anatase and rutile (TiO_2). Quartz (SiO_2) has a dominating role due to the strongly siliceous character of the Megalopolis ashes. No differences in the mineralogical investigation in relation to the chosen parameters were observed.

For the quantitative determination of the TiO_2 phases deposited onto the ash surfaces, X-ray diffraction patterns (XRD) of the calcinated powders were obtained in the diffraction angle range 2Θ=20-80° using Cu Kα radiation. Then, anatase/rutile percentages were calculated from the resulting diffracrograms using the Spurr-Myers equation [31]:

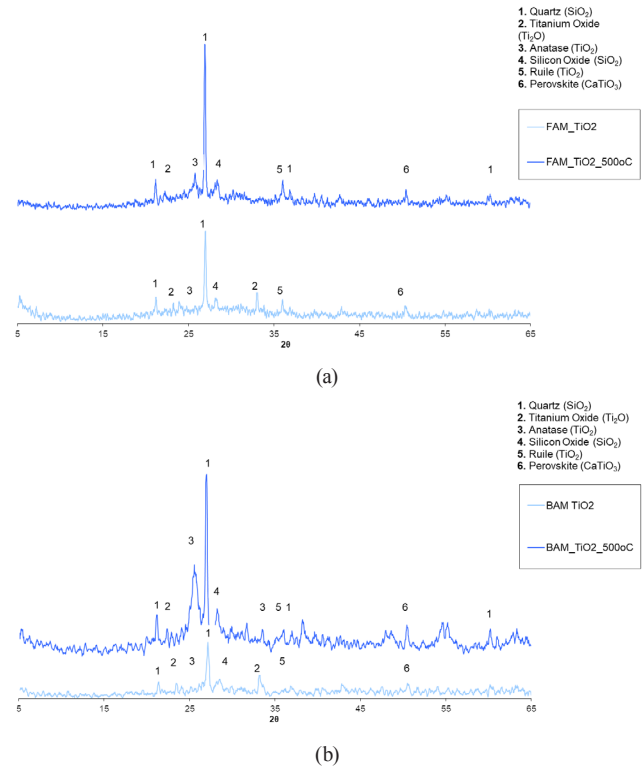$$\%_{Rutile} = \frac{1}{1+0.8\left[\dfrac{I_A(101)}{I_R(110)}\right]}.$$

Fig. 5 XRD spectra of non-sintered and sintered (500 °C - 2 h) (a) coated FAAD (b) coated BAAD

Fig. 6 XRD spectra of non-sintered and sintered (500 °C- 2 h) of (a) coated FAM (b) coated BAM

**Table 4** Rutile percentages calculated by Spurr-Myers equation

	As Received
FAAD (coated with TiO_2) sintered in 500 °C	63
BAAD (coated with TiO_2) sintered in 500 °C	55
FAM (coated with TiO_2) sintered in 500 °C	44
BAM (coated with TiO_2) sintered in 500 °C	43

where I_A is the intensity of (101) peak of anatase and I_R is the intensity of (110) peak of rutile structure.

In all TiO_2-coated ashes tested, the weight fraction of each crystal phase was calculated from the peak areas of the anatase (AA) and rutile (AR) peaks at 25.3° (2Θ) (101) and 27.5° (110) (2Θ) respectively. Furthermore, the rutile percentages are represented in Table 4.

Regarding the morphology of the specimens, a red tint colouring specifically for those prepared starting from Megalopolis ashes appeared, because of the transformation of Fe compounds to Fe_2O_3, as it was indicated by XRD. SEM micrographs (Fig. 7) reveal effectively densified microstructures, and differences due to the mineralogical phases and the granulometry of the ashes can be seen. The surface of the BAAD and BAM ashes coated with TiO_2 appears slightly more porous compared to that of the coated FAAD and FAM ones, which should be due to carbon burnout during sintering and also the existence of coarser particles. It should be mentioned that fly ashes contain not only dense solid but also hollow particles (cenospheres) that can be filled with TiO_2 during the process (e.g. Fig. 7 (b))EDX analysis, in fact, verified TiO_2 presence on cenospheres. Since cenospheres are consisted of glassy SiO_2, a better behavior of Ti in the absence of Ca may be indicated. It is also worthnoty that porosity may be desirable to attain weight reduction of the final products as well as for specific applications such as the treatment of a liquid wastes through a bed reactor filled with ashes.

The photocatalytic activity of TiO_2-coated ceramic substrates made of lignite ashes and thermally treated at 500 °C is illustrated in Fig. 8, which shows the methylene blue (MB) and methyl orange (MO) dye removal in aqueous solution as a function of irradiation time, under visible (cool daylight) and two types of UV-A light (blacklight and blacklight blue).

Concerning the experiments under visible light, a very intense decolorization of MB can be observed, while the highest activity is exhibited by the coated ceramic substrates made from FAAD, followed by those from bottom ash of the same power station.

Dye decomposition may partially be attributed to dye adsorption onto the porous and cracked coating on the ceramic substrate, taking into consideration the
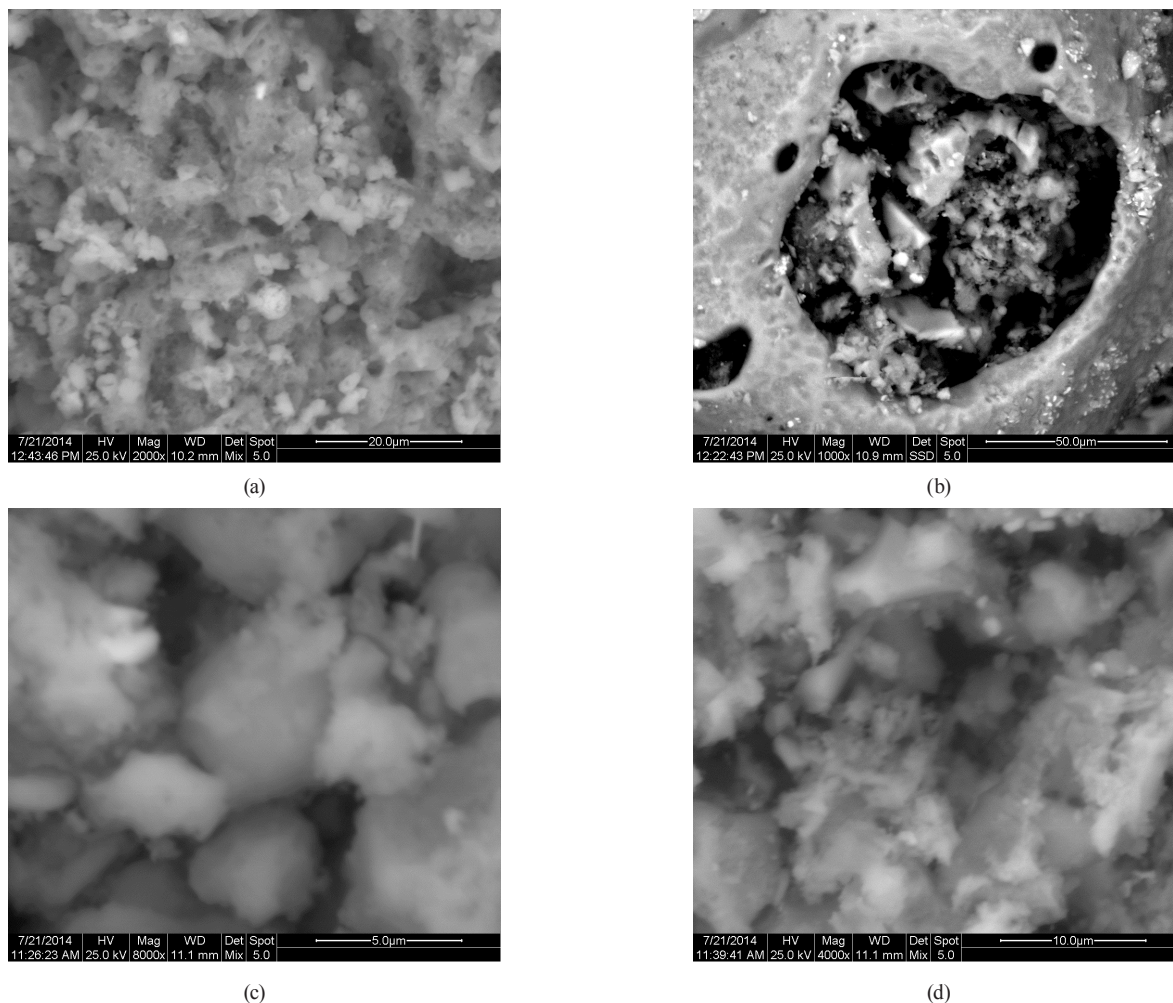
Fig. 7 SEM micrographs of sintered (500 °C, 2 h) coated with TiO_2 (a) FAAD, (b) BAAD, (c) FAM, and (d) BAM.
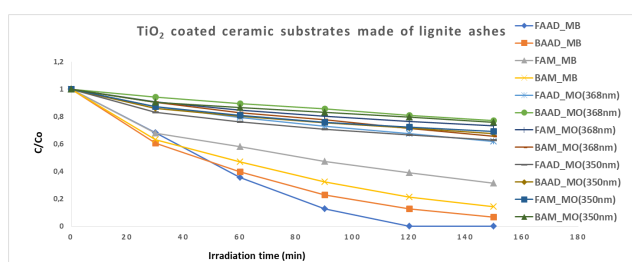
Fig. 8 Dye removal by the TiO_2-coated ceramic substrates made of lignite ashes, under visible and UV light, as a function of irradiation time.

aforementioned surface roughness results. It can, therefore, be assumed that during the experiments a combined mechanism takes place, which includes both adsorption and especially photodegradation phenomena.

On the other side, the removal of MO by the activated composite materials under the two types of UV-A irradiation, which is depicted in the same graph, is less pronounced than in the case of MB experiments. This finding should be correlated to the fact that the dye removal

efficiency depends on the pollutant itself, the irradiation type and other system parameters. Especially, high solution pH values encountered due to the alkaline nature of the ashes favor the adsorption of the cationic MB dye onto the substrate surface, whereas the removal of the anionic MO dye is negatively affected.

In Fig. 9, the dye removal results using the activated (TiO_2-coated) lignite ashes are graphically presented. Similarly to the coated ceramic substrates, the application of the activated lignite ash powders to the removal of MB under visible light leads to higher activity and thus higher dye decomposition compared to that of MO where no significant decolorization of the aqueous dye solution is demonstrated. Indeed, the highest MB removal rates are achieved for the two types of bottom ashes (BAAD and BAM), which is indicative of a better synergy of these two secondary materials examined, with TiO_2.

With regard to MO removal from the modified powdery lignite ashes, the obtained results are similar for the
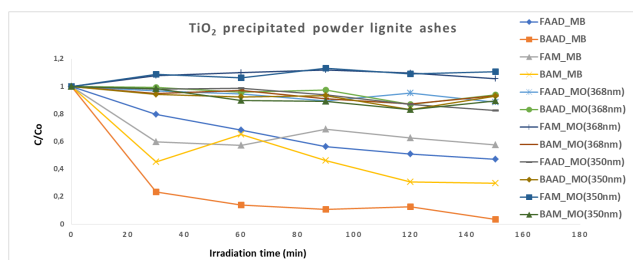
Fig. 9 Dye removal by lignite ash powders modified with TiO$_2$ precipitation, under visible and UV light, as a function of irradiation time.
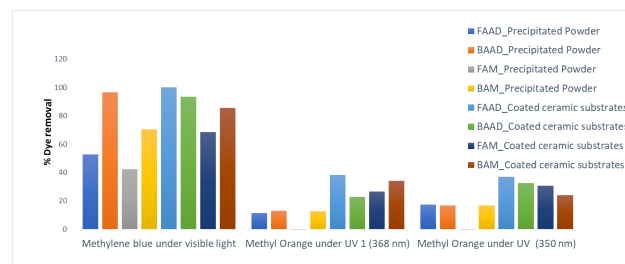
Fig. 10 Comparative % dye removal values for all the activated samples and experimental conditions

two types of UV-A irradiation but of fairly low efficiency. However, an interesting finding is that in all cases of the samples prepared from bottom ashes, the maximum dye removal was obtained at 120 min of irradiation and not at 150 min that as would be expected. This may be attributed to a possible desorption that takes place after a specific time.

The effectiveness of all composite materials produced for potential environmental applications, in terms of % pollutant (dye) removal efficiency, is summarized in Fig. 10, which provides an overall comparison. It is obvious from this graph that in all three dye/irradiation combinations examined, greater dye removal efficiency is generally demonstrated in the form of TiO$_2$-coated ceramic substrates rather than in the form of the activated lignite ash powders. The improved performance of the coated ceramic substrates may be explained by a higher adsorption capacity of the substrates and especially an enhanced photocatalytic activity of their TiO$_2$ film coating, promoting the dye decomposition [32].

4 Conclusions

Both calcareous and siliceous Greek lignite ashes, largely available power station by-products, were successfully transformed into composite materials with photocatalytic activity.

A comparison between a) ceramic substrates developed from the ashes and coated with TiO$_2$ film deposition and b) fly ash powders, surface modified with precipitation of TiO$_2$, reveals a greater pollutant (organic dye) removal photocatalytic efficiency for the TiO$_2$-coated ceramic substrates rather than for the activated lignite ash powders. This finding should be attributed to a higher dye adsorption capacity of the substrates mainly combined with an increased photocatalytic activity of the TiO$_2$ film coating.

Concluding, the results of the current research appear to be encouraging for further development of alternative value-added photocatalytic materials starting from industrial secondary resources, for their valorization in wastewater treatment in the context of circular economy.

References

[1] Feigl, V., Gruiz, K., Anton, A. "Remediation of metal ore mine waste using combined chemical- and phytostabilisation", Periodica Polytechnica Chemical Engineering, 54(2), pp. 71–80, 2010.
https://doi.org/10.3311/pp.ch.2010-2.03

[2] Baklavaridis, A. N., Samaras, P. E., Karayannis, V. G. "Recent progress in the advanced oxidation of wastewaters using recycled fly ashes as alternative catalytic agents", Desalination and Water Treatment, 133, pp. 292–306, 2018.
https://doi.org/10.5004/dwt.2018.23084

[3] Karamberi, A., Orkopoulos, K., Moutsatsou, A. "Synthesis of glass-ceramics using glass cullet and vitrified industrial by-products", Journal of the European Ceramic Society, 27(2-3), pp. 629–636, 2007.
https://doi.org/10.1016/j.jeurceramsoc.2006.04.126

[4] Nicoara, A. I., Badanoiu, A., Balanoiu, M., Mathias, A., Voicu, G. "Alkali Activated Mortars with Intumescent Properties", Revista de Chimie, 70(2), pp. 431–437, 2019.

[5] Savvilotidou, V., Kritikaki, A., Stratakis, A., Komnitsas, K., Gidarakos, E. "Energy efficient production of glass-ceramics using photovoltaic (P/V) glass and lignite fly ash", Waste Management, 90, pp. 46–58, 2019.
https://doi.org/10.1016/j.wasman.2019.04.022

[6] Tsimas, S., Moutsatsou-Tsima, A. "High-calcium fly ash as the fourth constituent in concrete: problems, solutions and perspectives", Cement and Concrete Composites, 27(2), pp. 231–237, 2005.
https://doi.org/10.1016/j.cemconcomp.2004.02.012

[7] Yao, Z. T., Ji, X. S., Sarker, P. K., Tang, J. H., Ge, L. Q., Xia, M. S., Xi, Y. Q. "A comprehensive review on the application of coal fly ash", Earth-Science Reviews, 141, pp. 105–121, 2015.
https://doi.org/10.1016/j.earscirev.2014.11.016

[8] Karayannis, V. G., Karapanagioti, H. K., Domopoulou, A. E., Komilis, D. P. "Stabilization/Solidification of Hazardous Metals from Solid Wastes into Ceramics", Waste and Biomass Valorization, 8(5), pp. 1863–1874, 2017.
https://doi.org/10.1007/s12649-016-9713-z

[9] Pergal, M. M., Relić, D., Tešić, Ž. L., Popović, A. R. "Leaching of polycyclic aromatic hydrocarbons from power plant lignite ash-influence of parameters important for environmental pollution", Environmental Science and Pollution Research, 21(5), pp. 3435–3442, 2014.
https://doi.org/10.1007/s11356-013-2314-5

[10] Tsiridis, V., Petala, M., Samaras, P., Kungolos, A., Sakellaropoulos, G. P. "Environmental hazard assessment of coal fly ashes using leaching and ecotoxicity tests", Ecotoxicology and Environmental Safety, 84, pp. 212–220, 2012.
https://doi.org/10.1016/j.ecoenv.2012.07.011

[11] Karayannis, V. G., Moustakas, K. G., Baklavaridis, A. N., Domopoulou, A. E. "Sustainable Ash-Based Geopolymers", Chemical Engineering Transactions, 63, pp. 505–510, 2018.
https://doi.org/10.3303/CET1863085

[12] Xu, G., Shi, X. "Characteristics and applications of fly ash as a sustainable construction material: A state-of-the-art review", Resources, Conservation and Recycling, 136, pp. 95–109, 2018.
https://doi.org/10.1016/j.resconrec.2018.04.010

[13] Belviso, C. "State-of-the-art applications of fly ash from coal and biomass: A focus on zeolite synthesis processes and issues", Progress in Energy and Combustion Science, 65, pp. 109–135, 2018.
https://doi.org/10.1016/j.pecs.2017.10.004

[14] Kioupis, D., Kavakakis, C., Tsivilis, S., Kakali, G. "Synthesis and Characterization of Porous Fly Ash-Based Geopolymers Using Si as Foaming Agent", Advances in Materials Science and Engineering, 2018, Article ID: 1942898, 2018.
https://doi.org/10.1155/2018/1942898

[15] Karayannis, V., Moutsatsou, A., Domopoulou, A., Katsika, E., Drossou, C., Baklavaridis, A. "Fired ceramics 100% from lignite fly ash and waste glass cullet mixtures", Journal of Building Engineering, 14, pp. 1–6, 2017.
https://doi.org/10.1016/j.jobe.2017.09.006

[16] Zhuang, X. Y., Chen, L., Komarneni, S., Zhou, C. H., Tong, D. S., Yang, H. M., Yu, W. H., Wang, H. "Fly ash-based geopolymer: clean production, properties and applications", Journal of Cleaner Production, 125, pp. 253–267, 2016.
https://doi.org/10.1016/j.jclepro.2016.03.019

[17] Adell, V., Cheeseman, C. R., Doel, A., Beattie, A., Boccaccini, A. R. "Comparison of rapid and slow sintered pulverised fuel ash", Fuel, 87(2), pp. 187–195, 2008.
https://doi.org/10.1016/j.fuel.2007.04.009

[18] Karamberi, A., Moutsatsou, A. "Vitrification of lignite fly ash and metal slags for the production of glass and glass ceramics", China Particuology, 4(5), pp. 250–253, 2006.
https://doi.org/10.1016/S1672-2515(07)60269-3

[19] Moutsatsou, A., Protonotarios, V. "Remediation of polluted soils by utilizing hydrothermally treated calcareous fly ashes", China Particuology, 4(2), pp. 65–69, 2006.
https://doi.org/10.1016/S1672-2515(07)60236-X

[20] Papandreou, A., Stournaras, C. J., Panias, D. "Copper and cadmium adsorption on pellets made from fired coal fly ash", Journal of Hazardous Materials, 148(3), pp. 538–547, 2007.
https://doi.org/10.1016/j.jhazmat.2007.03.020

[21] Dindi, A., Quang, D. V., Vega, L. F., Nashef, E., Abu-Zahra, M. R. M. "Applications of fly ash for CO_2 capture, utilization, and storage", Journal of CO_2 Utilization, 29, pp. 82–102, 2019.
https://doi.org/10.1016/j.jcou.2018.11.011

[22] Wang, S. "Application of Solid Ash Based Catalysts in Heterogenous Catalysis", Environmental Science and Technology, 42(19), pp. 7055–7063, 2008.
https://doi.org/10.1021/es801312m

[23] Wang, Y., He, Y., Lai, Q., Fan, M. "Review of the progress in preparing nano TiO_2: An important environmental engineering material", Journal of Environmental Sciences, 26(11), pp. 2139–2177, 2014.
https://doi.org/10.1016/j.jes.2014.09.023

[24] Katsanaki, A. B. "Φωτοκαταλυτική δράση νανοδομημένων οξειδίων του τιτανίου σε πρότυπους αντιδραστήρες αέριων ρύπων" (Photocatalytic activity of nanostructured titanium oxide materials in standardized reactors of air pollutants)", PhD thesis, National Technical University of Athens, 2012. (in Greek)

[25] Lei, X. F., Xue, X. X. "Preparation, characterization and photocatalytic activity of sulfuric acid-modified titanium-bearing blast furnace slag", Transactions of Nonferrous Metals Society of China, 20(12), pp. 2294–2298, 2010.
https://doi.org/10.1016/S1003-6326(10)60643-7

[26] Adam, F., Appaturi, J. N., Thankappan, R., Nawi, M. A. M. "Silica–tin nanotubes prepared from rice husk ash by sol–gel method: Characterization and its photocatalytic activity", Applied Surface Science, 257(3), pp. 811–816, 2010.
https://doi.org/10.1016/j.apsusc.2010.07.070

[27] Gilja, V., Katančić, Z., Krehula, L. K., Mandić, V., Hrnjak-Murgić, Z. "Efficiency of TiO_2 catalyst supported by modified waste fly ash during photodegradation of RR45 dye", Science and Engineering of Composite Materials, 26(1), pp. 292–300, 2019.
https://doi.org/10.1515/secm-2019-0017

[28] Shi, J. W., Chen, S. H., Wang, S. M., Wu, P., Xu, G. H. "Favorable recycling photocatalyst TiO_2/CFA: Effects of loading method on the structural property and photocatalytic activity", Journal of Molecular Catalysis A: Chemical, 303(1-2), pp. 141–147, 2009.
https://doi.org/10.1016/j.molcata.2009.01.016

[29] Frontistis, Z., Hapeshi, E., Fatta-Kassinos, D., Mantzavinos, D. "Ultraviolet-activated persulfate oxidation of methyl orange: A comparison between artificial neural networks and factorial design for process modelling", Photochemical & Photobiological Sciences, 14(3), pp. 528–535, 2015.
https://doi.org/10.1039/C4PP00277F

[30] Vlyssides, A. G., Papaioannou, D., Loizidoy, M., Karlis, P. K., Zorpas, A. A. "Testing an electrochemical method for treatment of textile dye wastewater", Waste Management, 20(7), pp. 569–574, 2000.
https://doi.org/10.1016/S0956-053X(00)00028-3

[31] Spurr, R. A., Myers, H. "Quantitative Analysis of Anatase-Rutile Mixtures with an X-Ray Diffractometer", Analytical Chemistry, 29(5), pp. 760–762, 1957.
https://doi.org/10.1021/ac60125a006

[32] Yetim, T., Tekin, T. "A Kinetic Study on Photocatalytic and Sonophotocatalytic Degradation of Textile Dyes", Periodica Polytechnica Chemical Engineering, 61(2), pp. 102–108, 2017.
https://doi.org/10.3311/PPch.8535